Size Dependence of the Atomic Distributions and Oxygen Reduction Reaction Catalytic Activity in PtCu Octahedral Nanocrystals

Shlomi Polani,[†] Meital Shviro,[‡,⊥] Victor Shokhen, [†] Marcelo Carmo,[⊥] Andreas Glüsen,[⊥] Rafal Dunin-Borkowski,[‡] and David Zitoun[†,*]

†Department of Chemistry, Bar-Ilan Institute for Technology and Advanced Materials (BINA), Bar-Ilan University, Ramat Gan, 5290002, Israel

‡Ernst Ruska-Centre for Microscopy and Spectroscopy with Electrons and Peter Grünberg Institute, Forschungszentrum Jülich GmbH, 52425 Jülich, Germany

⊥Institute of Electrochemical and Climate Research IEK-3, Forschungszentrum Jülich GmbH, 52425 Jülich, Germany

Abstract

The synthetic control through colloidal synthesis led to remarkable increase in platinum mass activity in octahedral nanocrystals with Pt rich surface. In this manuscript, we demonstrate that the ratio of surfactant can tune the size of Pt surface enriched PtCu nano-octahedra from 8 to 18 nm with homogeneous size and shapes on carbon support. For the nano-octahedra, the Pt-rich surface has been established by high-angle annular dark field scanning transmission electron microscopy and energy-dispersive X-ray spectroscopy. The Pt rich surface exhibits an increasing compressive strain with increasing surface of the {111} facets. With increasing surface, the PtCu nano-octahedra display higher oxygen reduction reaction (ORR) activity. This observed trend for a series of size selected nano-octahedra demonstrates the benefits of extending well-defined {111} Pt surface for the ORR activity.

KEYWORDS: octahedral nanoparticles, Pt-Cu, electrocatalysis, oxygen reduction reaction, PEMFCs

Proton-exchange membrane fuel cells (PEMFCs) have been the focus of attention for many years, and the main issue remains the quest for a performant, cost-effective and durable electrocatalyst for the complex oxygen reduction reaction (ORR). The standard catalyst, which is used in relatively high loading in the cathodes of fuel cells, consisting of active carbons decorated with in situ grown Pt or Pt alloys nanoparticles (NPs). A significant limitation for commercialization of this technology is the high loading of Pt, while another catalytic limitation arises from the high overpotential at which the ORR takes place on Pt/C NPs.[1] To improve the activity of electrocatalysts for the ORR, the materials-by-design strategy where the design relies on the results obtained on well-defined surfaces and segregation-induced thin layers has been highly successful.[2] Early studies on the kinetics of Pt single-crystal planes for the ORR are found to vary with the crystallographic orientation. Amongst the three low index faces, the activity increases in the order of (100) < (110) = (111).[3] Studies conducted on Pt-based extended surfaces show volcano-type behavior on the ORR activity, where the alloying of Pt with the 3d-transition metals or lanthanides enhances the ORR activity.[4–7] These surfaces are highly active due to the formation of segregated Pt-skin and Pt-skeleton strained surfaces with a down-shifted d-band center relative to pure Pt. The electrocatalytic trends established for extended surfaces are useful to provide a fundamental basis to explain the activity pattern of Pt-based nanocatalysts. Controlling the surface structure of Pt and Pt-based NPs has been studied to maximize their catalytic efficiency by selecting the exposed crystal facets and composition for the intended reaction.[8] Furthermore, dealloying processes where the less noble metal is dissolved allow control over surface composition. Dealloying can be achieved through different means such as annealing, electrochemical or chemical treatment.[9–17] The Pt-enriched surface layers supported on an alloy core with a smaller lattice parameter display a strain in the shell. Bimetallic NPs structure can display Pt-rich surfaces and the atomic spatial distribution is highly dependent on the reaction conditions.[18–20] It is well known that the shape of the NPs influences the catalytic properties due to the specific surface atomic arrangement and coordination.[21,22] Shape-controlled synthesis of Pt-based nanocrystals has been widely studied, leading to the development of multiple strategies to control the shapes of Pt-based nanocrystals with diverse compositions.[23–26] Strategies have focused on manipulating the exposed facets by employing specific shape-directing agents. CuPt octahedral NPs have been reported in literature, with shape-directing agents such as CTAB,[27] CTAC,[28] I^-,[29] and CO gas.[30] The effect of different precursor-ligand couples has been investigated[30] and ternary CuPtM (M=Pd and Ni) has been synthesized as well.[31,32] To the best of our knowledge, this is the first synthesis of well-defined Cu@Pt/C octahedral morphology bounded by {111} facets with a robust and selective synthesis of Cu@Pt/C octahedral NPs with different sizes.

Here, we report a highly efficient strategy for one-pot synthesis of well-defined PtCu octahedral nanocrystals dispersed on carbon in which both the size and number of platinum layers on the surface are

tunable. PtCu octahedral NPs with size ranging from 8 to 18 nm have been prepared by adjusting the amount of CTAB, while the other synthesis parameters remain unchanged. The successful fabrication of crystalline-controlled PtCu octahedral nanocrystals with identically exposed facets and same compositions provides an ideal case for studying the size effect of the {111} facets on ORR electrocatalysis. We found that all the PtCu octahedra exhibit higher electrocatalytic activities for the ORR than commercial Pt/C; the ORR specific activity increasing with the particle size.

Results and discussion

CuPt octahedral nanocrystals were prepared using $Pt(acac)_2$ and $Cu(acac)_2$ in dimethylformamide with benzoic acid and cetyltrimethylammonium bromide (CTAB), which act as capping agents, using a solvothermal method as described in the experimental section. Tuning the amount of CTAB itself was a facile and robust way to achieve control over size. TEM images (Figure S1) show the homogeneity of the CuPt octahedral shape and their corresponding narrow particle size distribution (PSD). CuPt octahedral NPs uniformly dispersed on high-surface area carbon supports with sizes of 8, 10, 14 and 18 nm (vertex-to-vertex along the <100> direction) were prepared by employing 5, 10, 15 and 20 mg of CTAB respectively, under otherwise constant conditions. In the following, the samples are labeled as PtCu-S where S means the vertex-to-vertex particle size in nm along the ⟨100⟩ direction.

In Figure S3, the dependency of particle mean size on the amount of CTAB is presented, the linear fit show a slope of 0.66 mg/nm and interception at 4.7 nm corresponding to the size of NPs synthesized without CTAB. The formation of Cu@Pt/C crystalline octahedral is evident from high-angle annular dark field scanning transmission electron microscopy (HAADF-STEM) images (Figure 1). All the particles with different sizes display a bright outline, which is visible along the edges and corners of the octahedra and may be attributed to the atomic contrast.

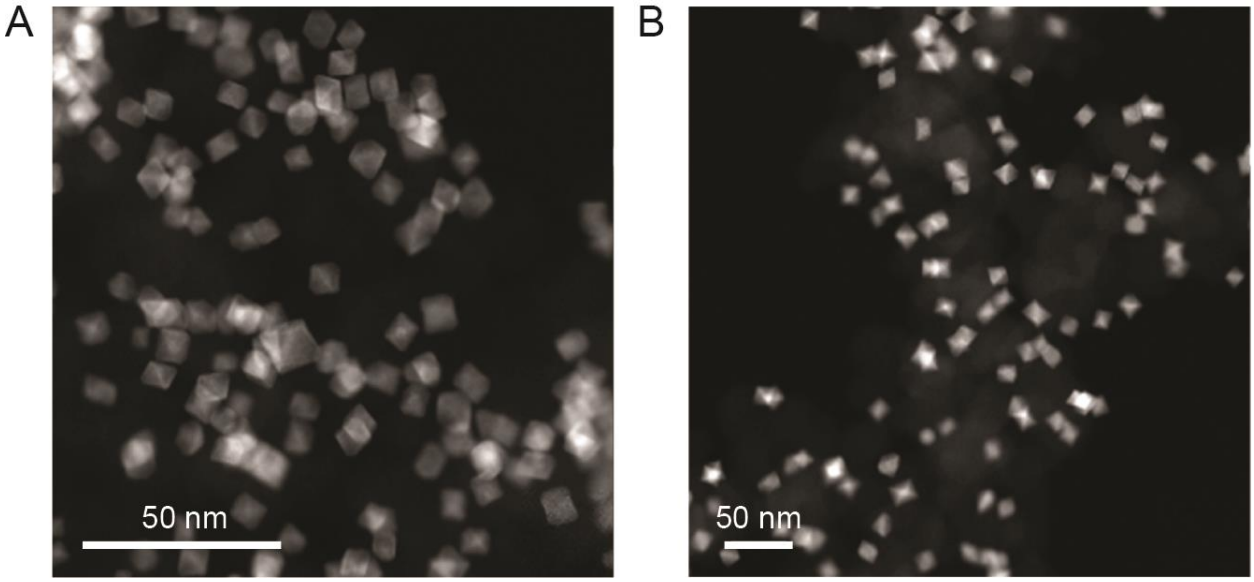

Figure 1. HAADF-STEM images of Cu@Pt/C octahedral NPs of 10 nm (PtCu-10) (A) and 18 nm (PtCu-18) (B)

To further explore the intensity differences in the HAADF-STEM images, we investigated the particles with STEM-EDS spectrum imaging. All these NPs showed a uniform morphology with composition ratio Pt/Cu=1. The elemental maps of the PtCu-8 and PtCu-10 show platinum-rich surface and copper-rich core (figure 2A-B), which is in agreement with the HAADF-STEM images. STEM-EDS line analysis was applied as shown in Figure S2A-B, the platinum and copper atomic distributions were studied in octahedral NPs oriented along the (100) zone axes. Line scans along the (110) direction started and ended at the edges, passing through the central octahedron axis. The relative intensities showed a clear Pt enrichment on the surface compared to Cu-rich core. From the intensity of the elemental line profiles, the platinum and copper segregation occurs close to the nanoparticle edge (Figure S2A-B). The elemental segregation observed with the formation of a platinum-rich surface is consistent with the observations reported by Strasser et al on inhomogeneous bimetallic nanoparticles after dealloying.[9] The relative lower standard reduction potential of copper leads to the metal etching on the surface of the NPs through galvanic replacement by the Pt^{n+} species and possible oxidative etching in solution. Different nucleation windows of the components and adsorbate induced segregation can lead to surface enrichment as well. In the PtCu system, a positive segregation energy should drive Cu to the surface ($\Delta E_{(Cu)Pt}$ = 0.41eV).[33] However, as observed for most of the Pt based bimetallic particles, the system seems to be driven by the presence of surface ligands, namely benzoic acid, which preferentially coordinate and leach out the Cu surface atoms.

Upon increase of CTAB, the PtCu system still shows a Pt rich surface with a slightly different atomic distribution. PtCu-14 and PtCu-18 display Pt rich edges, as observed from EDX mapping (Fig. 2C-D). STEM-EDS line analysis was also applied as shown in Figure S2C-D, the platinum and copper atomic distributions were studied in octahedral NPs oriented along the (100) zone axes. The relative intensities showed a clear Pt enrichment in the edges and corners.

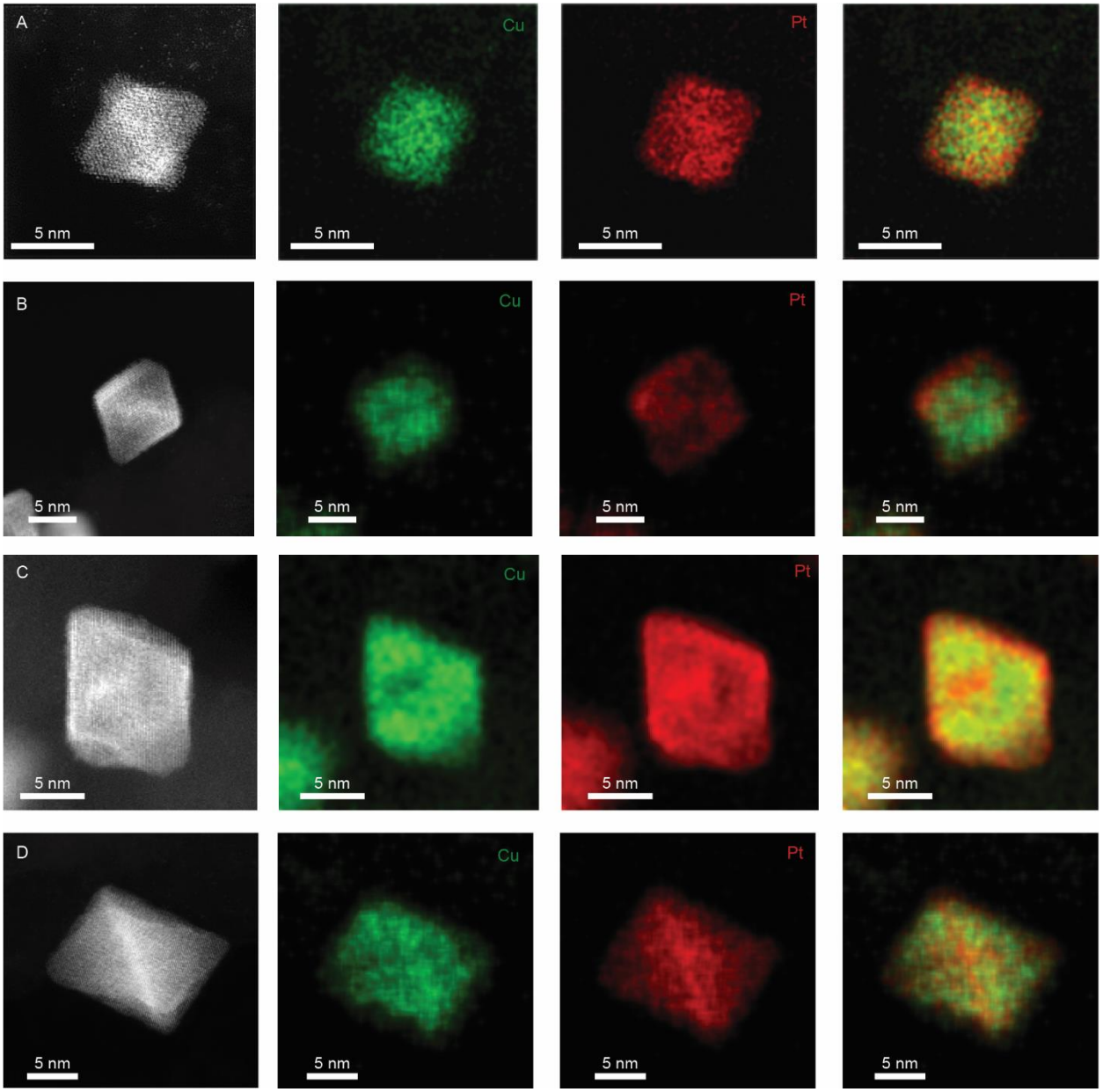

Figure 2. HAADF-STEM images and EDS line scan, EDS elemental mapping of Cu, EDS elemental mapping of Pt and their overlay for PtCu-8, PtCu-10, PtCu-14, PtCu-18 (panels A-D respectively)

The XRD patterns indicate that the PtCu NPs are single crystal face-centered cubic (FCC) structure with {111} interplane distance in between that of pure Pt (2.26 Å) and Cu (2.09 Å). The XRD patterns for the NPs synthesized with different amount of CTAB also show a sharpening of the peaks, which is consistent with the increase in particle size (Figure 3A). We observe a shoulder of the (111) peak at $2\theta \sim 42^{o}$ (named as peak 1). This asymmetry is due to a broader secondary peak at the lower 2θ, arising from the Pt-rich surface. The asymmetry is more visible on the PtCu-8 sample (Fig. 3B) and diminishes as the particles size increases.

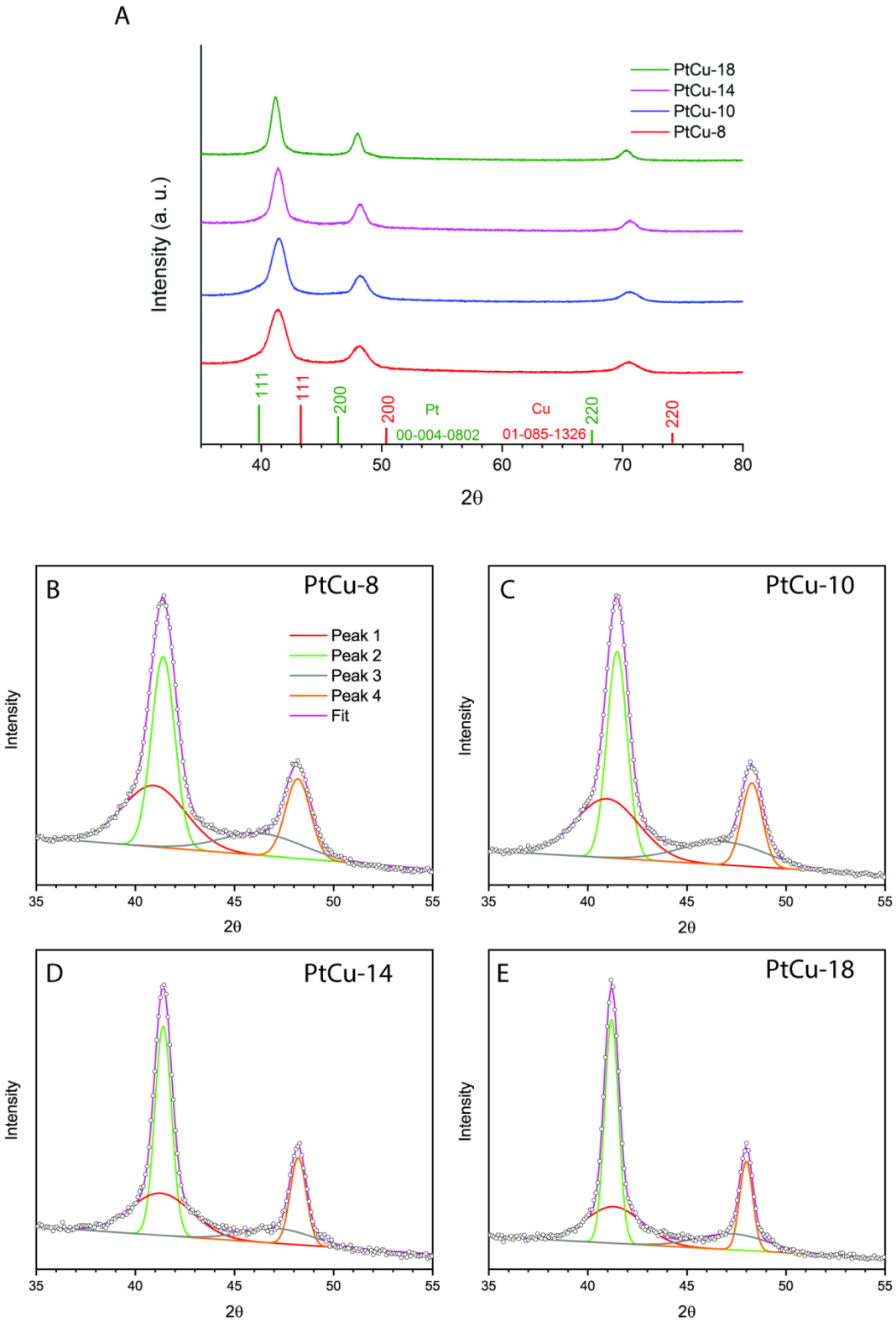
A
PtCu-18
PtCu-14
PtCu-10
PtCu-8
Intensity (a. u.)
111
111
200
200
Pt
Cu
220
220
00-004-0802
01-085-1326
40
50
60
70
80
2θ
B
PtCu-8
Peak 1
Peak 2
Peak 3
Peak 4
Fit
Intensity
35
40
45
50
55
2θ
C
PtCu-10
Intensity
35
40
45
50
55
2θ
D
PtCu-14
Intensity
35
40
45
50
55
2θ
E
PtCu-18
Intensity
35
40
45
50
55
2θ

Figure 3. XRD patterns of PtCu octahedral NPs (A); deconvolution of the (111) and (200) Bragg reflections for PtCu-8 to Pt-Cu-18 (B-E respectively)

Figure 3B-E show the fitting of typical profiles of the different particles sizes; two Gaussian functions fit well the (111) and (200) reflections of all of the samples. For the (111) reflection, the two peaks are identified as peak one which corresponds to the Pt-rich shell and peak two which correspond to the Cu-rich core. For the (200) reflection, the two peaks are identified as peak three and peak four. The peaks centers are shifted to smaller unit cells from PtCu-8 to PtCu-18, which suggests that the Pt-rich shell in PtCu-8 displays lattice parameters close to the platinum unit cell (1.4% smaller lattice parameter than bulk Pt). With increasing size of the nano-octahedra, the assymetry of the peaks almost disappears and the XRD deconvolution shows two contributions with the same lattice parameter (3% smaller lattice parameter than bulk Pt). Regarding PtCu-8 and PtCu-10 with a clear Cu core- Pt shell structure, it implies that the Pt rich shell exhibits a compressive strain of 1.4% and 2.2% respectively. For larger samples, where the surface is mixed with Pt edges and Cu facets, the compressive strain is higher and reaches 3% for PtCu-14 and PtCu-18. The XRD results are in agreement with the EDX results and suggest the interplay between particle size, and number of Pt layers on the surface in our case study. Comparable asymmetry has been described for dealloyed $PtCu_3$ films by Yang et al.[12] and for octahedral M@Pt (M = Cu or Ni) by LaGrow et al.[30]

In the absence of CTAB, the PtCu octahedral NPs could not be formed, only spherical NPs with smallest particle size of 4.6 ± 0.6 nm and a pure Pt composition according to the EDX results (Figure 4). The XRD pattern shows the presence of a Cu pure phase with much sharper Bragg reflections than that of the Pt phase (Figure 4A), which is consistent with slow formation of large Cu nanoparticles that could not be observed by TEM. To further explore the role of CTAB in the synthesis, we reacted $Cu(acac)_2$ alone into two vials, the first contains only DMF while the second contains DMF and CTAB. After heating the vials to 160°C, we observe the formation of Cu nanoparticles after half an hour in the absence of CTAB and 4 hours in the presence of CTAB. The slow kinetics in the presence of CTAB explain the finding that CTAB concentration directly correlate to the NPs sizes, since the slow reaction kinetics yield fewer nucleation centers and therefore larger particles. Moreover, only the presence of CTAB can direct the formation of uniform and monodisperse octahedral nanocrystals by slowing down the reaction kinetics, while unshaped particles are formed in the absence of it (Figure 4B). These results clearly suggest a kinetic role played by CTAB, which can change the reduction rate and nucleation window of Cu complexes by forming micelles[34] and subsequently acts as a capping agent.[35] The octahedral shape itself can be explained by the stabilization of the {111} facets of Pt or Pt-rich surfaces in the presence of bromide ligand.[25,36,37]

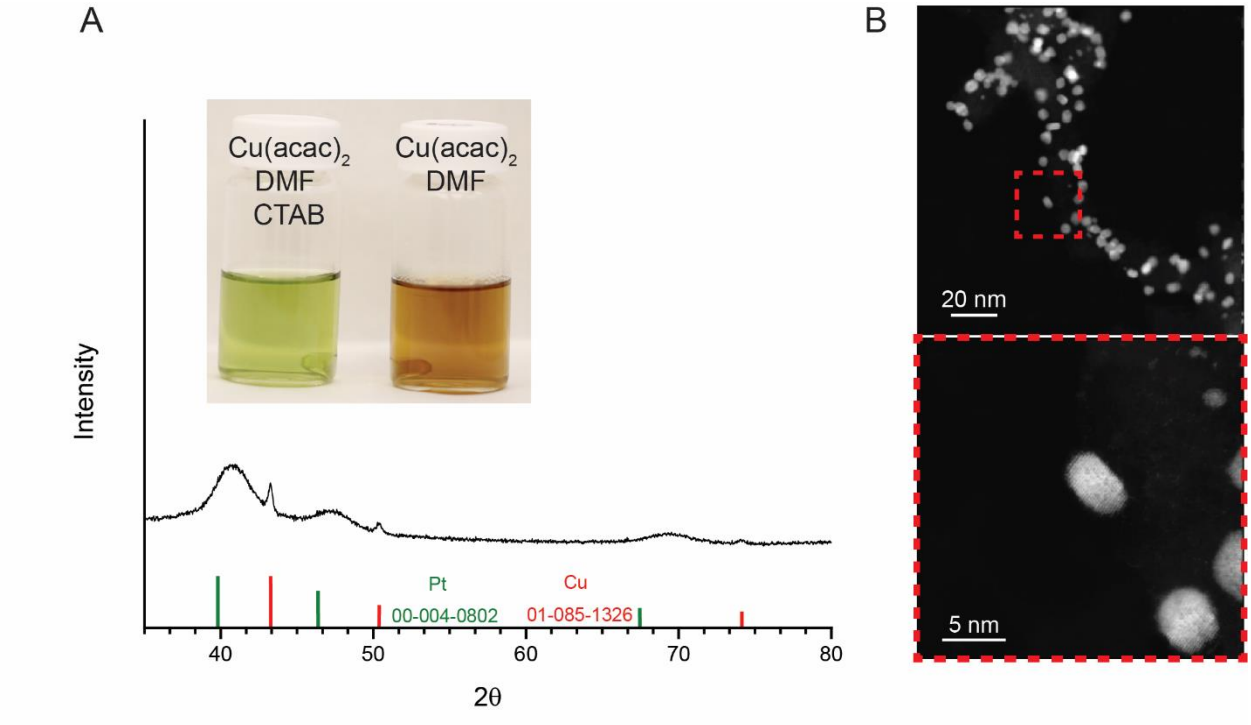

Figure 4. XRD of the synthesis without CTAB (A), photographs of the vials after reaction (inset) and HAADF-STEM images of the Pt nanoparticles obtained without CTAB (B)

For the electrocatalytic study, we recorded cyclic voltammetry (CV) at 298 K in 0.1 M $HClO_4$ solution at a sweep rate of 100 mV/s (Figures 5A and S4A). The electrochemical surface areas (ECSAs) was calculated from the H_{UPD} and reach the values of 26.82, 30.23, 18.69 and 20.75 $m^2\ g^{-1}$ for PtCu-8, CuPt-10, PtCu-14 and PtCu-18 respectively and 116.2 m^2/g for the standard catalyst (Pt/C 20% from Johnson-Mattey, named Pt JM in the following). Figure 5B shows the ORR polarization curves of PtCu-8, PtCu-18 nm and Pt JM carried out in an oxygen-saturated 0.1 M $HClO_4$ solution at a sweep rate of 10 mV/s and at a rotation rate of 1600 rpm (for PtCu-10 and PtCu-14 see figure S4B). From the polarization curves, the calculated kinetic current density at 0.9 and 0.95 V were normalized over the Pt loading weight and ECSA to give the mass activity and specific activity, respectively (Figure 5C-D). We found that the catalytic specific and mass activities of all PtCu octahedral are greater than those of Pt JM. At 0.9 V, the PtCu-8 showed a specific activity of 1.38 mA cm^{-2} and a mass activity of 0.34 mA mg_{Pt}^{-1}, a 6.9 times higher specific activity and 2 times mass activity enhancement compared to Pt JM (0.2 mA cm^{-2} and 0.17 mA mg_{Pt}^{-1}). With increasing size, the mass activity remains constant while the specific activity slightly increases to 1.58 mA cm^{-2} for the PtCu-18 octahedra.

The main result concerns the increasing trend in ORR onset potential observed with increasing vertex-to-vertex length of the octahedra. The activity enhancement is demonstrated by the specific activity trend at 0.95 V. The PtCu-18 showed a specific activity of 0.83 mA cm^{-2} and mass activity of 0.065 mA mg_{Pt}^{-1}. We found that the specific activity of the PtCu-18 is two times higher than the PtCu-8 and reveals the global trend of increasing specific activity for extended {111} facets. Compared to previously reported specific activities, the CuPt-8 display the same activity as the Pt_3Cu octahedral NPs with similar size reported by Sun et al[27] and Cu@Pt strained NPs.[9]

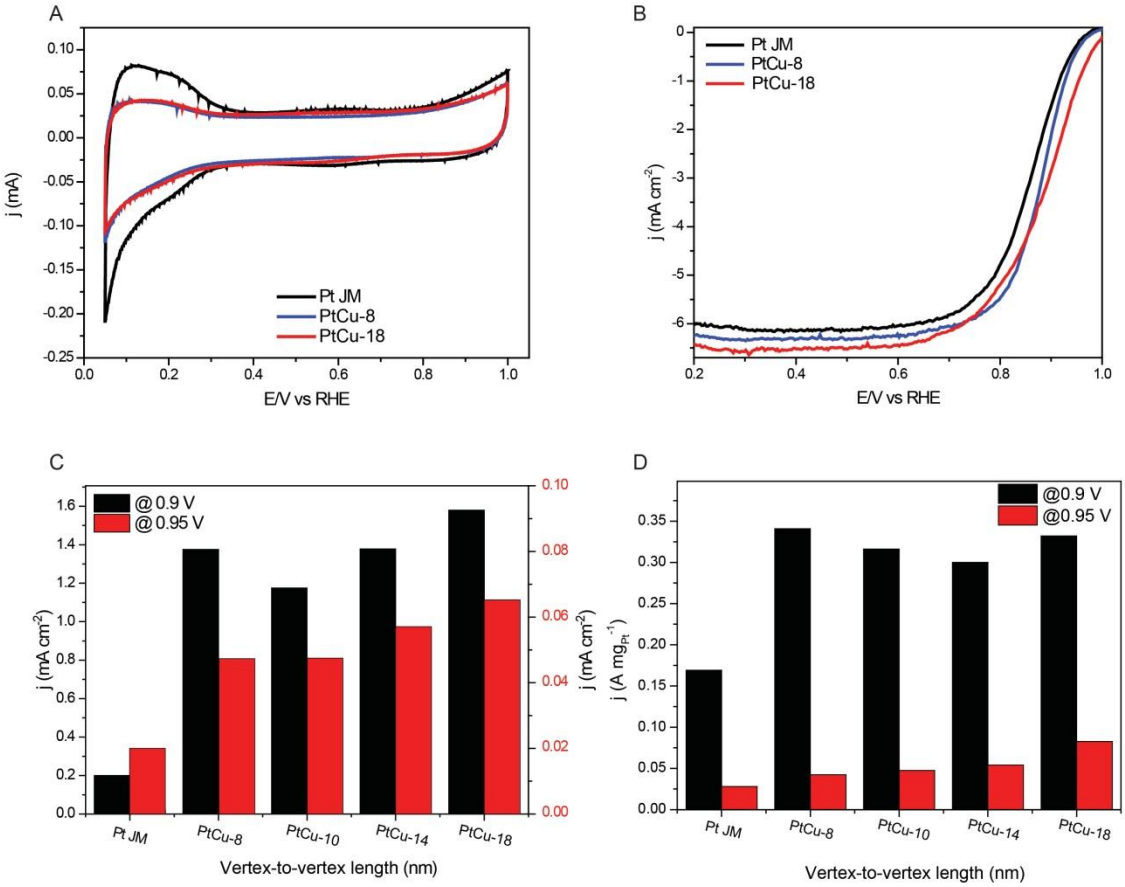

Figure 5. CVs recorded at room temperature in an Ar-saturated and 0.1 M $HClO_4$ solution with a sweep rate of 100 mV s^{-1} (A). ORR polarization curves recorded at room temperature in an O_2-saturated 0.1 M $HClO_4$ aqueous solution with a sweep rate of 10 mV s^{-1} and a rotation rate of 1600 rpm (B). Specific and mass activity for the ORR at 0.9 and 0.95 V for all of the catalysts (C and D respectively).

The size and shape-controlled of PtCu octahedra gave us a chance to observe the influence of the size on the atomic distribution of Cu and Pt, and subsequently on the ORR activity. First, all the octahedra display only {111} facets with a Pt rich surface for all the particles sizes of the study. Second, the copper

core determines the compressive strain on the Pt surface. As the particle size grows, the Pt surface displays an increasing compressive strain up to 3 % for PtCu-18. Indeed, in the case of a few layers of Pt surface, the compressive-strain effects has been shown to be responsible for the high activity of the NPs and we can exclude the role of the vicinity of a second metal (so called ligand effect) due to the limited range of this effect.[38]

Qualitatively, the ORR activity scales with the strain of the Pt surface. The highest ORR activity was measured on the 3% strained Pt surface (PtCu-18). For smaller size, like PtCu-10, the measured strained is only 1.4% which could explain the lower ORR activity. The thickness of the Pt layer can be estimated from the line scan, together with the HAADF-STEM image. The Pt surface consists of 4 atomic layers for PtCu-10. These two values (1.4% strain for 4 atomic Pt layers) quantitatively match the DFT calculations predicting the relationship between the layer thickness, the strain and the oxygen binding energy.[9]

Conclusion

The present work suggests a synthetic approach for controlling the size of the active facets and thus to improve the electrocatalytic performance of ORR electrocatalysts. The addition of CTAB surfactant in a single step colloidal synthesis of carbon supported copper-platinum nanocrystals promote the formation of nano-octahedra. The addition of surfactant leads to the linear increase of the octahedra size from 8 to 18 nm with a high homogeneity in size and shape. The HAADF-STEM combined with EDS demonstrates the Pt rich surface on a Cu core which results in compressive strain on the Pt layers. The increasing ORR specific activity observed with size seems to origin from the high compressive stress. The ability to control size and shape in the PtCu octahedra activity through the simple addition of a non-binding surfactant offers an excellent model to observe the trend in structure-activity relationship. Indeed, we could attribute the increase of the ORR activity to the optimized compressive strain of the Pt surface.

Methods

Materials. platinum(II) acetylacetonate ($Pt(acac)_2$, 97%), nickel(II) acetylacetonate ($Ni(acac)_2$, 95%), benzoic acid (C_6H_5COOH, ≥99.5%), N, N-dimethylformamide (DMF, ≥99.9%), Cetyltrimethylammonium bromide (CTAB, 99%) and Nafion (Wt% 5) were all purchased from Sigma-Aldrich. Commercial Pt/C Johnson Matthey (JM, 20 wt% Pt). Carbon black (C, Vulcan XC72R carbon) purchased from Cabot Corporation. All the chemicals were used as received without further purification.

Synthesis of Cu@Pt/C octahedral NPs. In a typical synthesis of octahedral Cu@Pt/C catalyst, 10 mg $Pt(acac)_2$, 6.6 mg $Cu(acac)_2$, 60 mg benzoic acid, 10 mL carbon black dispersed in DMF (2 mg/mL) and

CTAB amount corresponding to the desired particles size were added into a vial. After the vial had been capped, the mixture was ultrasonicated for 15 minutes. The resulting homogeneous mixture was then heated to 160 °C for 12 h, before it was allowed to cool down to room temperature. The resulting colloidal products were collected by centrifugation and washed three times with an ethanol/acetone mixture. Cu@Pt/C octahedral catalyst with 8, 10, 14 and 18 nm (vertex to vertex along the <100> direction) were synthesized by adding 5, 10, 15 and 20 mg of CTAB respectively. Synthesis of spherical Pt/C was done in the absence of CTAB.

Characterization

Morphological, structural, and elemental characterization

The structure of the NPs is investigated using transmission electron microscopes (TEM): JEOL 1400 at 120 kV. The high-angle annular dark-field scanning transmission electron microscopy (HAADF-STEM) micrographs and electron dispersive spectroscopy (EDS) maps were acquired using a monochromated and double corrected Titan Themis G2 60-300 (FEI / Thermo Fisher) operated at 300KeV and equipped with a DualX detector (Bruker). The quantitative analysis of the EDS maps was done using the Velox software (FEI / Thermo Fisher). Scanning TEM (STEM) was performed at 200 kV on an FEI Titan 80-200 ("ChemiSTEM") TEM,[39] equipped with a C_S -probe corrector (CEOS GmbH) and a high-angle annular dark field (HAADF) detector operated at 200 kV. To achieve "Z-Contrast" conditions, a probe semi-angle of 25 mrad and an inner detector collection semi-angle of the detector of 88 mrad were used. EDX Compositional maps were obtained using four symmetric large-solid-angle silicon drift detectors. For EDX measurement an FEI double-tilt holder was used, and the TEM specimen was untilted. EDX analysis was performed using ESPRIT software (Bruker Company, Berlin, Germany) using the Cu and Pt L peaks. The crystalline phases and crystallinity of the prepared powders were examined by XRD using Cu Ka (0.1541 nm) radiation (Bruker Advance D8).

Electrochemical measurements

A typical three-electrode cell was used to perform the electrochemical measurements. The working electrode was a glassy carbon rotating disk electrode (RDE) (0.196 cm^2, Pine Instrument). A hydrogen reference electrode (Gaskatel, HydroFlex) and Pt wire was used as counter electrode. A catalyst ink was prepared by mixing the as-prepared catalyst Cu@Pt/C powder in ethanol, water, and Nafion (5%) (v/v/v = 8:2:0.01) and sonicated for 45 min in an ice bath. 7.5 microliters of the catalyst ink were cast on an RDE and dried under ambient conditions. The loading amount of metal Pt for the 8, 10, 14 and 18 Cu@Pt/C octahedral catalysts were 1.7, 2.2, 3.2 and 2.9 μg_{pt} respectively. For comparison, Commercial Pt/C catalyst JM was used as the baseline catalysts with a Pt loading of 10.2 $\mu g_{Pt}/cm^2$. Cyclic voltammetry

(CV) measurements were conducted in a 0.1 M $HClO_4$ argon-saturated solution with a potential scan rate of 100 mV/s. Oxygen reduction reaction (ORR) measurements were conducted in a 0.1 M $HClO_4$ solution which was purged with oxygen during the measurement. The scan rate was 10 mV/s and the ORR polarization curves were collected at 1600 rpm. The ECSAs were determined by integrating the hydrogen adsorption charge on the CV.

ASSOCIATED CONTENT

Supplementary Information

The Electronic Supplementary Information includes

The Supplementary Information is available free of charge on the website.

AUTHOR INFORMATION

Corresponding author

*E-mail: David.Zitoun@biu.ac.il

Competing interests

The authors declare no competing financial interests.

REFERENCES AND NOTES

(1) Gasteiger, H. A.; Kocha, S. S.; Sompalli, B.; Wagner, F. T. Activity Benchmarks and Requirements for Pt, Pt-Alloy, and Non-Pt Oxygen Reduction Catalysts for PEMFCs. *Appl. Catal. B Environ.* **2005**, *56* (1–2 SPEC. ISS.), 9–35.

(2) Stamenkovic, V. R.; Strmcnik, D.; Lopes, P. P.; Markovic, N. M. Energy and Fuels from Electrochemical Interfaces. *Nat. Mater.* **2016**, *16* (1), 57–69.

(3) Markovic, N. Kinetics of Oxygen Reduction on Pt(Hkl) Electrodes: Implications for the Crystallite Size Effect with Supported Pt Electrocatalysts. *J. Electrochem. Soc.* **1997**, *144* (5), 1591.

(4) Stamenkovic, V. R.; Mun, B. S.; Arenz, M.; Mayrhofer, K. J. J.; Lucas, C. A.; Wang, G.; Ross, P. N.; Markovic, N. M. Trends in Electrocatalysis on Extended and Nanoscale Pt-Bimetallic Alloy Surfaces. *Nat. Mater.* **2007**, *6* (3), 241–247.

(5) Stamenkovic, V.; Mun, B. S.; Mayrhofer, K. J. J.; Ross, P. N.; Markovic, N. M.; Rossmeisl, J.; Greeley, J.; Nørskov, J. K. Changing the Activity of Electrocatalysts for Oxygen Reduction by Tuning the Surface Electronic Structure. *Angew. Chemie Int. Ed.* **2006**, *45* (18), 2897–2901.

(6) Lindahl, N.; Zamburlini, E.; Feng, L.; Grönbeck, H.; Escudero-Escribano, M.; Stephens, I. E. L.;

Chorkendorff, I.; Langhammer, C.; Wickman, B. High Specific and Mass Activity for the Oxygen Reduction Reaction for Thin Film Catalysts of Sputtered Pt3Y. *Adv. Mater. Interfaces* **2017**, *4* (13), 1–9.

(7) Escudero-Escribano, M.; Malacrida, P.; Hansen, M. H.; Vej-Hansen, U. G.; Velazquez-Palenzuela, A.; Tripkovic, V.; Schiotz, J.; Rossmeisl, J.; Stephens, I. E. L.; Chorkendorff, I. Tuning the Activity of Pt Alloy Electrocatalysts by Means of the Lanthanide Contraction. *Science (80-.).* **2016**, *352* (6281), 73–76.

(8) Strasser, P. Catalysts by Platonic Design. *Science (80-.).* **2015**, *349* (6246), 379–380.

(9) Strasser, P.; Koh, S.; Anniyev, T.; Greeley, J.; More, K.; Yu, C.; Liu, Z.; Kaya, S.; Nordlund, D.; Ogasawara, H.; Toney, M. F.; Nilsson, A. Lattice-Strain Control of the Activity in Dealloyed Core-Shell Fuel Cell Catalysts. *Nat. Chem.* **2010**, *2* (6), 454–460.

(10) Srivastava, R.; Mani, P.; Hahn, N.; Strasser, P. Efficient Oxygen Reduction Fuel Cell Electrocatalysis on Voltammetrically Dealloyed Pt-Cu-Co Nanoparticles. *Angew. Chemie - Int. Ed.* **2007**, *46* (47), 8988–8991.

(11) Mani, P.; Srivastava, R.; Strasser, P. Dealloyed Pt-Cu Core-Shell Nanoparticle Electrocatalysts for Use in PEM Fuel Cell Cathodes. *J. Phys. Chem. C* **2008**, *112* (7), 2770–2778.

(12) Yang, R.; Leisch, J.; Strasser, P.; Toney, M. F. Structure of Dealloyed PtCu3 Thin Films and Catalytic Activity for Oxygen Reduction. *Chem. Mater.* **2010**, *22* (16), 4712–4720.

(13) Mani, P.; Srivastava, R.; Strasser, P. Dealloyed Binary PtM3 (M=Cu, Co, Ni) and Ternary PtNi3M (M=Cu, Co, Fe, Cr) Electrocatalysts for the Oxygen Reduction Reaction: Performance in Polymer Electrolyte Membrane Fuel Cells. *J. Power Sources* **2011**, *196* (2), 666–673.

(14) Oezaslan, M.; Hasché, F.; Strasser, P. PtCu3, PtCu and Pt3Cu Alloy Nanoparticle Electrocatalysts for Oxygen Reduction Reaction in Alkaline and Acidic Media. *J. Electrochem. Soc.* **2012**, *159* (4), B444.

(15) Coleman, E. J.; Chowdhury, M. H.; Co, A. C. Insights into the Oxygen Reduction Reaction Activity of Pt/C and PtCu/C Catalysts. *ACS Catal.* **2015**, *5* (2), 1245–1253.

(16) Li, M.; Li, M.; Zhao, Z.; Cheng, T.; Fortunelli, A.; Chen, C.; Yu, R.; Gu, L.; Merinov, B.; Lin, Z.; Zhu, E.; Yu, T.; Jia, Q.; Guo, J.; Zhang, L.; Iii, W. A. G.; Huang, Y.; Duan, X. Ultrafine Jagged Platinum Nanowires Enable Ultrahigh Mass Activity for the Oxygen Reduction Reaction. *Science (80-.).* **2016**, *259* (1994), In Press.

(17) Wang, D.; Yu, Y.; Xin, H. L.; Hovden, R.; Ercius, P.; Mundy, J. A.; Chen, H.; Richard, J. H.; Muller, D. A.; Disalvo, F. J. Tuning Oxygen Reduction Reaction Activity via Controllable Dealloying: A Model Study of Ordered Cu3Pt/C Intermetallic Nanocatalysts | EFRC Community Website. *Nano Lett.* **2012**, *12* (10), 5230.

(18) Cui, C.; Gan, L.; Heggen, M.; Rudi, S.; Strasser, P. Compositional Segregation in Shaped Pt Alloy Nanoparticles and Their Structural Behaviour during Electrocatalysis. *Nat. Mater.* **2013**, *12* (8), 765–771.

(19) Gan, L.; Cui, C.; Heggen, M.; Dionigi, F.; Rudi, S.; Strasser, P. Element-Specific Anisotropic Growth of Shaped Platinum Alloy Nanocrystals. *Science (80-.).* **2014**, *346* (6216), 1502–1506.

(20) Ortiz, N.; Weiner, R. G.; Skrabalak, S. E. Ligand-Controlled Co-Reduction versus Electroless Co-Deposition: Synthesis of Nanodendrites with Spatially Defined Bimetallic Distributions. *ACS Nano* **2014**, *8* (12), 12461–12467.

(21) Tian, N.; Zhou, Z. Y.; Sun, S. G. Platinum Metal Catalysts of High-Index Surfaces: From Single-Crystal Planes to Electrochemically Shape-Controlled Nanoparticles. *J. Phys. Chem. C* **2008**, *112* (50), 19801–19817.

(22) Kang, Y.; Yang, P.; Markovic, N. M.; Stamenkovic, V. R. Shaping Electrocatalysis through Tailored Nanomaterials. *Nano Today* **2016**, *11* (5), 587–600.

(23) Porter, N. S.; Wu, H.; Quan, Z.; Fang, J. Shape-Control and Electrocatalytic Activity-Enhancement of Pt-Based Bimetallic Nanocrystals. *Acc. Chem. Res.* **2013**, *46* (8), 1867–1877.

(24) Wu, J.; Yang, H. Platinum-Based Oxygen Reduction Electrocatalysts. *Acc. Chem. Res.* **2013**, *46* (8), 1848–1857.

(25) Wang, J.; Li, B.; Yersak, T.; Yang, D.; Xiao, Q.; Zhang, J.; Zhang, C. Recent Advances in Pt-Based Octahedral Nanocrystals as High Performance Fuel Cell Catalysts. *J. Mater. Chem. A* **2016**, *4*, 11559–11581.

(26) Bele, M.; Jovanovič, P.; Pavlišič, A.; Jozinović, B.; Zorko, M.; Rečnik, A.; Chernyshova, E.; Hočevar, S.; Hodnik, N.; Gaberšček, M. A Highly Active $PtCu_3$ Intermetallic Core–shell, Multilayered Pt-Skin, Carbon Embedded Electrocatalyst Produced by a Scale-up Sol–gel Synthesis. *Chem. Commun.* **2014**, *50* (86), 13124–13126.

(27) Sun, X.; Jiang, K.; Zhang, N.; Guo, S.; Huang, X. Crystalline Control of {111} Bounded Pt_3Cu Nanocrystals: Multiply-Twinned Pt_3Cu Icosahedra with Enhanced Electrocatalytic Properties. *ACS Nano* **2015**, *9* (7), 7634–7640.

(28) Jia, Y.; Su, J.; Chen, Z.; Tan, K.; Chen, Q.; Cao, Z.; Jiang, Y.; Xie, Z.; Zheng, L. Composition-Tunable Synthesis of Pt–Cu Octahedral Alloy Nanocrystals from PtCu to $PtCu_3$ via Underpotential-Deposition-like Process and Their Electro-Catalytic Properties. *RSC Adv.* **2015**, *5* (23), 18153–18158.

(29) Lu, B. A.; Sheng, T.; Tian, N.; Zhang, Z. C.; Xiao, C.; Cao, Z. M.; Ma, H. Bin; Zhou, Z. Y.; Sun, S. G. Octahedral PtCu Alloy Nanocrystals with High Performance for Oxygen Reduction Reaction and Their Enhanced Stability by Trace Au. *Nano Energy* **2017**, *33*, 65–71.

(30) LaGrow, A. P.; Knudsen, K. R.; AlYami, N. M.; Anjum, D. H.; Bakr, O. M. Effect of Precursor Ligands and Oxidation State in the Synthesis of Bimetallic Nano-Alloys. *Chem. Mater.* **2015**, *27* (11), 4134–4141.

(31) Zhang, C.; Sandorf, W.; Peng, Z. Octahedral Pt2CuNi Uniform Alloy Nanoparticle Catalyst with High Activity and Promising Stability for Oxygen Reduction Reaction. *ACS Catal.* **2015**, *5* (4), 2296–2300.

(32) Mao, J.; Cao, T.; Chen, Y.; Wu, Y.; Chen, C.; Peng, Q.; Wang, D.; Li, Y. Seed-Mediated Synthesis of Hexameric Octahedral PtPdCu Nanocrystals with High Electrocatalytic Performance. *Chem. Commun.* **2015**, *51* (84), 15406–15409.

(33) Wang, L. L.; Johnson, D. D. Predicted Trends of Core-Shell Preferences for 132 Late Transition-Metal Binary-Alloy Nanoparticles. *J. Am. Chem. Soc.* **2009**, *131* (39), 14023–14029.

(34) Cierpiszewski, R.; Hebrant, M.; Szymanowski, J.; Tondre, C. Copper (II) Complexation Kinetics with Hydroxyoximes in CTAB Micelles Effect of Extractant Hydrophobicity and Additives. *J. Chem. Soc., Faraday Trans.* **1996**, *92* (2), 249–255.

(35) Wu, S. H.; Chen, D. H. Synthesis of High-Concentration Cu Nanoparticles in Aqueous CTAB Solutions. *J. Colloid Interface Sci.* **2004**, *273* (1), 165–169.

(36) Yoon, D.; Park, S.; Park, J.; Kim, J.; Baik, H.; Yang, H.; Lee, K. One Pot Synthesis of Hollow Cu-Doped Ru Octahedral Nanocages via an in Situ Generated Metastable Cu Nanoparticle Template. *Nanoscale* **2014**, *6* (21), 12397–12402.

(37) Xia, B. Y.; Ng, W. T.; Wu, H. Bin; Wang, X.; Lou, X. W. Self-Supported Interconnected Pt Nanoassemblies as Highly Stable Electrocatalysts for Low-Temperature Fuel Cells. *Angew. Chemie - Int. Ed.* **2012**, *51* (29), 7213–7216.

(38) Schlapka, A.; Lischka, M.; Groß, A.; Käsberger, U.; Jakob, P. Surface Strain versus Substrate Interaction in Heteroepitaxial Metal Layers: Pt on Ru(0001). *Phys. Rev. Lett.* **2003**, *91* (1), 016101/1-016101/4.

(39) Kovács, A.; Schierholz, R.; Tillmann, K. FEI Titan G2 80-200 CREWLEY. *J. large-scale Res. Facil. JLSRF* **2016**, *2* (0), A43.

Graphical abstract